Real-Time Nanomechanical and Topographical Mapping on Live Bacterial Cells-Brevibacterium casei under Stress Due to Their Exposure to Co2+ Ions during Microbial Synthesis of Co3O4...

ARTICLE *in* THE JOURNAL OF PHYSICAL CHEMISTRY B · JUNE 2009

Impact Factor: 3.3 · DOI: 10.1021/jp902698n · Source: PubMed

3 AUTHORS:

Umesh Kumar
The Energy and Resources Institute
13 PUBLICATIONS **135** CITATIONS
SEE PROFILE

Vivekanand Kalaparthi
Tufts University
8 PUBLICATIONS **174** CITATIONS
SEE PROFILE

Pankaj Poddar
CSIR - National Chemical Laboratory, Pune
134 PUBLICATIONS **2,408** CITATIONS
SEE PROFILE

Real-Time Nanomechanical and Topographical Mapping on Live Bacterial Cells—*Brevibacterium casei* under Stress Due to Their Exposure to Co^{2+} Ions during Microbial Synthesis of Co_3O_4 Nanoparticles

Umesh Kumar,[†] K. Vivekanand,[†] and Pankaj Poddar*

Materials Chemistry Division, National Chemical Laboratory, Pune-411008, India

Received: March 25, 2009

The study of elastic properties of microbial and mammalian cells using atomic force microscopy, with force-sensitivity as high as pico-Newtons and spatial resolution of a few nanometers, is proving to be a great tool for the real-time observation of the effects of drugs, biomolecules, metal ions, and nanoparticles on cell physiology in their natural environment. It has been shown that the Young's modulus of the cell surfaces is extremely sensitive to the surrounding environment. Recently, a broad array of microbes have been used successfully to synthesize nanocrystals of several metal and metal oxides in a controlled manner at room temperature after exposing them to various metal ion precursors. However, so far there is no report on the fate of their elastic properties and cell topography etc. during and after their exposure to the metal ions during the microbial synthesis of nanomaterials. Additionally, this information is also found to be extremely relevant to areas such as bioremediation, bioleaching, and biomineralization, where it is important to study the direct influence on the cell physiology in the presence of metal ions. Here, we report, for the first time, the use of AFM force−distance curves on live cells, to directly monitor (in real time) the changes in the surface-topography, surface-adhesion, indentation-depth, and Young's modulus of a metal-tolerant marine bacterium, *Brevibacterium casei,* isolated from the coast of the Arabian Sea, after its exposure to the Co^{2+} ions during the process of biosynthesis of nanoparticles. We earlier reported that this bacterium is capable of using the cobalt acetate as a precursor to synthesize protein-functionalized Co_3O_4 nanoparticles with very high crystallinity. Our study indicates a significant change in the morphology as well as elastic and adhesive properties of the *Brevibacterium casei*, where we found an increase in the adhesive properties and the indentation depth of the bacterial surfaces and a decrease in the cell stiffness after several hours of exposure to the cobalt acetate. We have discussed both qualitative and quantitative analysis of the force-spectroscopy data in detail.

Introduction

In the last two decades, there has been phenomenal growth in the development of wet-chemical methods to synthesize nanomaterials such as semiconductor quantum-dots, noble metals, ferromagnetic and ferroelectric materials, etc. However, despite the success in achieving excellent control over the size and shape, there are efforts to reduce or eliminate the hazards involved in these processes to human health and the environment through research on alternative green synthesis methods by learning from nature. The biomimetic approaches of the controlled synthesis of nanomaterials based on the use of microbes are fast gaining popularity where the microbes participate via reduction, oxidation, or hydrolysis of the transition metal ion precursors and also by acting as templates. These methods also overcome the problems related to the requirements of high pressure, temperature, extreme pH conditions, hazardous chemicals, and expensive organometallic precursors that are usually associated with the chemical synthesis methods. The as-synthesized nanomaterial surfaces in microbial synthesis methods are inherently functionalized by proteins and other biomolecules which not only facilitate further linking to the other ligands but also provide much needed surface passivation, prevention from agglomeration, and stable suspension in the aqueous medium, which are often difficult to address in the wet-chemical approaches.

Usually, in these microbial methods, metal precursors (mostly acetates and nitrates) which are often toxic are fed to the selected metal ion tolerant microbes (bacteria, fungi, yeast). These microbes convert the metal ions into their nontoxic forms, either intracellularly or extracellularly, in their natural habitat.[1−4] So far, microbial techniques have been used to synthesize a range of metal[5] and binary oxides[6−8] (TiO_2, SiO_2, ZrO_2, Fe_3O_4) as well as a few ternary oxides. Recently, Bansal et al. reported the fungus mediated synthesis of the barium titanate ($BaTiO_3$) with an average particle size of 5 nm in the stable tetragonal ferroelectric phase at room temperature.[2] Additionally, the reported work of Umesh et al. is perhaps the first example of extracellular synthesis of protein-functionalized ferromagnetic Co_3O_4 nanocrystals by the marine bacterium *Brevibacterium casei*, using cobalt acetate as a precursor, where the bacterium is directly involved in changing the oxidation state of Co from 2^+ to 3^+ (by synthesizing Co_3O_4 nanoparticles instead of CoO or Co nanoparticles), which is energetically an unfavorable reaction.[1] The biochemical pathways of reactions, which might be involved in this transition, are yet to be explored and quite challenging to answer. Besides this, it has to be determined whether the formation of Co^{3+} from Co^{2+} ions, during the synthesis of Co_3O_4 nanoparticles, implies that they are less toxic to the bacterium. Additionally, it is always important to know

* Corresponding author e-mail: p.poddar@ncl.res.in.
† U.K. and K.V. have contributed equally to the work.

10.1021/jp902698n CCC: $40.75
Published on Web 05/12/2009

the effect of the Co^{2+} environment during the biosynthesis, on the live bacterial cells (the change in the cell topography, elasticity, plasticity, and adhesiveness etc.). Earlier, based on the scanning electron microscope imaging, we showed that *Brevibacterium* tends to aggregate together to form clusters after exposing them to the cobalt acetate, even though the bacterium that we selected was tolerant to the Co-ion toxicity for the concentration of the Co-ions that we used for the synthesis of Co_3O_4 nanoparticles.[1] However, our previous scanning electron microscopy imaging was done after fixing the cells using gluteraldehyde and did not show the morphology of the live cells. It should be noted that, so far, there is no direct live-cell imaging study in the literature to investigate the effect of metal ion toxicity on the bacterial cells during the microbial synthesis which requires tools such as atomic force microscopy or environmental scanning electron microscopy.

Recently, atomic force microscopy (AFM) has turned out to be the instrument of choice to image cells in their physiological environment both statically and dynamically. AFM is currently the only technique that can image the surface of a living cell down to molecular level resolution and in real time. Thus, its importance in the surface science of cellular systems is well beyond being just a complementary technique to electron microscopy for topographical mapping. The main advantage of using AFM at a relatively lower resolution (micrometer level) is that the dynamic events, such as the cell growth, budding processes, and changes in the cell surface morphology resulting from the treatment with external agents (e.g., enzymes and antibiotics), can be directly tracked in real time, providing a wealth of information. In this technique, either the bacterium is attached to the AFM tip[9] or the tip is used to probe the bacterium.[10] Additionally, using force spectroscopy (force−distance curves), it is possible to precisely get quantitative information about elasticity, plasticity, adhesiveness, and the indentation-depth of the materials, including polymers, biological materials, thin films, etc. at the nanolevel.[11] In simpler words, it is a record of the controlled approach and interaction of the tip and sample where the force involved such as the electrostatic, magnetostatic, van-der Waals, capillary, and adhesive forces, etc. can be probed at a level down to the pico-Newton. As we indicated earlier, the potential of AFM for stable imaging as well as the acquisition of force−distance curves on the living cells for extended time periods facilitates the study of dynamic processes due to the external stimuli, which is not possible by any other method. In simple language, the AFM technique relies on a basic principle where a sample attached to a piezoelectric positioner is rastered beneath a sharp tip attached to a sensitive cantilever spring. Undulations in the surface lead to the deflection of the cantilever, which is monitored optically using a photodiode. Usually, a feedback loop is employed, which keeps the cantilever deflection constant, and the corresponding movement of the piezoelectric positioner thus generates the image.[12−14]

There are several reports in the literature, where the force−distance spectroscopy has been extensively and successfully used to locally measure the elastic properties of cellular systems using it as a nanoindentation technique.[15−21] It is now understood that the stiffness of a cell surface, as observed by the indentation with an AFM tip, may originate from various sources such as (a) the cell wall itself and/or (b) underlying structures (cytoskeleton etc.) and/or (c) the pressure difference between the cell interior and the exterior. Arnoldi et al. presented a theoretical model, taking into account different contributions to measure the cell stiffness by osmotic pressure inside the bacterium (turgor pressure), the bending elasticity of the cell wall, and the surface tension. The application of this model to the indentation curves on the bacterium *Magnetospirillum gryphiswaldense* showed that the measured cell response is dominated by the turgor pressure of 10^5 Pa. Similar values of the turgor pressure were also found for the *Pseudomonas aeruginosa* and *Enterococcus hirae* bacteria.[22] It is reported in the literature that for the live mammalian cells, for example, liver endothelial cells, the typical values of the elastic modulus are around 2 kPa and more than 100 kPa for the gluteraldehyde fixed cells.[23] Various groups have seen a similar effect for the *E. coli* K12 strains, where a 4-fold increase in the cell stiffness was found due to the cell fixation.[10] Higher values of the Young's modulus were also reported for isolated sheaths of the archeaon *Methanospirrilum hungatei* GP1 (20−40 GPa).[24] In fact, the force-plot measurements can also be used to differentiate between the normal cells and the cancerous cells.[25] It was reported that in the case of living lung carcinoma cells, Young's modulus ranges from 0.013 to 0.1 MPa[16] whereas in the human platelets this value is in the range of 1−50 kPa.[17] In the case of prokaryotic cells such as *B. subtillis*, the value of Young's modulus is as high as 50 MPa whereas, in the case of eukaryotic cells such as *S. cerevisiae*, it is up to 110 MPa.[26] Hence, due to the sensitive nature of this technique, we have used this technique to answer a few of the fundamental questions related to the cell-mechanism during the biosynthesis after exposure to the Co^{2+} ions.

Below we present our results on the force−distance spectroscopy to understand the effect of Co^{2+} exposure during the synthesis of Co_3O_4 nanocrystals on the *Brevibacterium* cells. A detailed quantitative and qualitative analysis of the changes in the nanomechanical properties of cells such as Young's modulus, indentation depth, and adhesiveness is discussed.

Results and Discussion

For the atomic force microscopy measurements, the bacterial cells were grown in the Zobell broth and harvested after they were fully grown. These cells were washed twice with Millipore water by centrifuging the cells at 6000 rpm for 5 min. Finally, these cells were suspended in Millipore water and drop-casted on the freshly cleaved mica substrates for the AFM measurements. For the real time observation of the Co^{2+} ion toxicity effects on the cells, the cells were incubated with an aqueous solution of cobalt acetate. In this case, the concentration of the cobalt acetate was kept similar to the concentration which was used in our earlier study for the synthesis of Co_3O_4 nanoparticles using the *Brevibacterium casie* culture.[1] The cells were drop-casted on the mica surfaces after 24, 48, and 72 h of incubation to study a time dependent effect on the cell physiology, and these results were compared with those of the untreated cells (control i.e. 0 h). Therefore, our study truly represents the changes in the morphology and mechanical properties during as well as after the biosynthesis of the Co_3O_4 nanoparticles. Here, the 0 h measurement corresponds to the time prior to reaction, the sample taken after 24 h of incubation corresponds to the measurements "during" the synthesis process and the corresponding surface changes on bacterial cells, and the 48 h sample represent the time-scale after completion of the synthesis process and reflects the corresponding surface changes. Lastly, the 72 h sample corresponds to the time interval well beyond the formation of nanoparticles.

The atomic force microscopy measurements were performed using a Multimode scanning probe microscope equipped with a Nanoscope IV controller from Veeco Instrument Inc., Santa

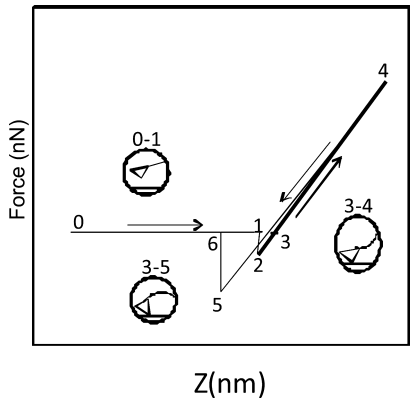

Figure 1. Schematic of a typical force−distance curve showing various parts of the interactions in the approach and retract cycles.

Barbara, CA. All the AFM measurements were done under ambient conditions using the soft tapping mode AFM probes model-Multi75Al purchased from Budget Sensors, with proper precautions to avoid drying of the cells. The radii of tips used in this study were less than 100 nm, and their height was 17 μm. The probe used had a resonant frequency of 75 kHz with a 30 nm thick aluminum reflex coating on the back side of the cantilever of the length 225 μm, and it was characterized for the force constant using the thermal noise method[27] using a Nanoscope V controller from Veeco Instruments. The measured force constant was around 1.86 N/m (soft enough for the biological cells). It is worth mentioning here that it is important to measure the exact value of the force constant to convert the cantilever deflection and tip−sample distance curve into the force−distance curve. The soft cantilevers are susceptible to thermal fluctuations, which can be measured and analyzed (cantilever movement) by AFM. The thermal noise spectrum is a plot of cantilever fluctuations as a function of frequency; usually the greatest amplitude will be seen around the cantilever resonance frequency, where there will be a maximum energy transfer. The amplitude of fluctuations at a given temperature depends entirely upon the spring-constant of the cantilever;[28] therefore, the thermal resonance curve can be fitted into a Lorentz function which allows calculation of the spring-constant. The deflection sensitivity of the cantilever was calibrated at the end of the measurements by drawing a line parallel to the 2−4 segment of a typical force plot curve (Figure 1), where the tip is already in contact with the hard surface, obtained on a freshly cleaned silicon substrate which converts the cantilever deflection value, which is generated in Volt units from the photodiode detectors, to distance units (the actual cantilever deflection in nanometers). The calibration on the hard surfaces ensures that the indentation depth is zero while doing the deflection sensitivity measurements. The deflection sensitivity is different for each cantilever and changes with the cantilever length, thickness, coating, and contamination, etc. It should be noted that the cantilever sensitivity also depends on the position of the laser light on the cantilever as well as the quality of the laser beam reflection (spot size, shape) from the cantilever. Here we took all the precautions possible to have reproducible deflection sensitivity.

The schematic in Figure 1 shows the loading and unloading cycle during force−distance measurements. As shown in the schematic, in the region 0−1, when the tip starts approaching the sample surface and the separation between them is approximately 10−100 μm, there is no interaction between the tip and the sample. Typically, for a tip−sample separation of a few micrometers to a few tens of nanometers, the long-range electrostatic forces contribute to the approach part of a force−distance curve. When the separation reduces to below a few tens of nanometers, magnetostatic, van der Waals, capillary, and other short-range forces play a predominant role, shown by region 0−1 in the schematic, just before the jump into contact point. At around position 1, when the tip−sample separation is hardly a few atomic distances, the tip comes into contact with the sample. Position 1 is also called the jump-into-contact point, where the tip is pulled toward the sample due to the capillary, van der Waals forces. The 3−4 segment of the schematic represents the event when the tip presses into the sample surface and the cantilever bends upward. This region is very informative, as it gives an idea of the stiffness (Young' modulus, elastic or plastic response, and viscoelastic response, etc.) of the sample. The segment 4−6 shows that the tip is lifting-off the sample surface (a few atomic distances to nanometers). This region gives an idea about the adhesive properties of the sample, which can be specific (ligand−receptor) or nonspecific (chemical affinity, surface coatings, etc.). Precisely, the 5−6 segment of the schematic shows the point where the tip leaves contact with the surface. This is also known as jump-off contact. It gives an idea of the adhesive forces, as we shall discuss in this paper.[11] It can be noticed that almost each part of the force−distance curves carries significant and precise information about the tip−sample interaction.

In Figure 2 (top panel), we have shown the surface topography of the untreated (not exposed to the Co^{2+} ions) live cells assembled on the mica surface in a 5 μm range using the cantilever deflection image (error signal mode), where we could observe a nice closed packed structure of the microbial cells without any visible surface deformation or damage. In the lower panel of the same figure, we have shown the section analysis on the untreated cells where the average size of the cells is ∼1.2 μm. It is worth mentioning that, in the microbial imaging, due to the roughness of the samples, generally, the deflection image provides much detailed information in comparison to the height image; therefore, we chose to present only the deflection images.

In Figure 3, we have compared the surface topography of the cells incubated with the cobalt acetate. The top, middle, and bottom panels show the topography (deflection) images after 24, 48, and 72 h of interaction with the cobalt ions during the Co_3O_4 synthesis, respectively. We did not capture the image after 72 h, as this is the maximum time required for the complete synthesis of Co_3O_4 nanoparticles. In comparison to the earlier image shown in Figure 2 (for the untreated cells), we can see a remarkable deformation in the cellular structure associated with the aggregation of the cells, which increases as a function of time (from 24 to 72 h) due to the increasing exposure of the Co^{2+} ions on the cells during the synthesis process. In our earlier paper, we explained the mechanism behind the aggregation and deformation of the cells in response to the precursor salts (1 mM cobalt acetate) in detail.[1] We believe that this is a kind of stress response where many bacterial strains produce excess extracellular exopolysaccharide or slime or form capsules to protect themselves against the metal ions.[1] Capsules, slime, and bacterial acidic exoploysaccharide are known to bind and concentrate metal ions and are therefore thought to play a considerable role in ameliorating metal toxicity.[29,30] These secondary metabolites enforce isolated cells to clump together to form aggregates.[31] It is believed that in these self-organized colonies bacterium can be more resistive to the external stress in comparison to the suspension. Once under the external stress (such as metal ions, food scarcity, antibiotics, adverse environmental conditions, etc.) the bacteria communicate with each

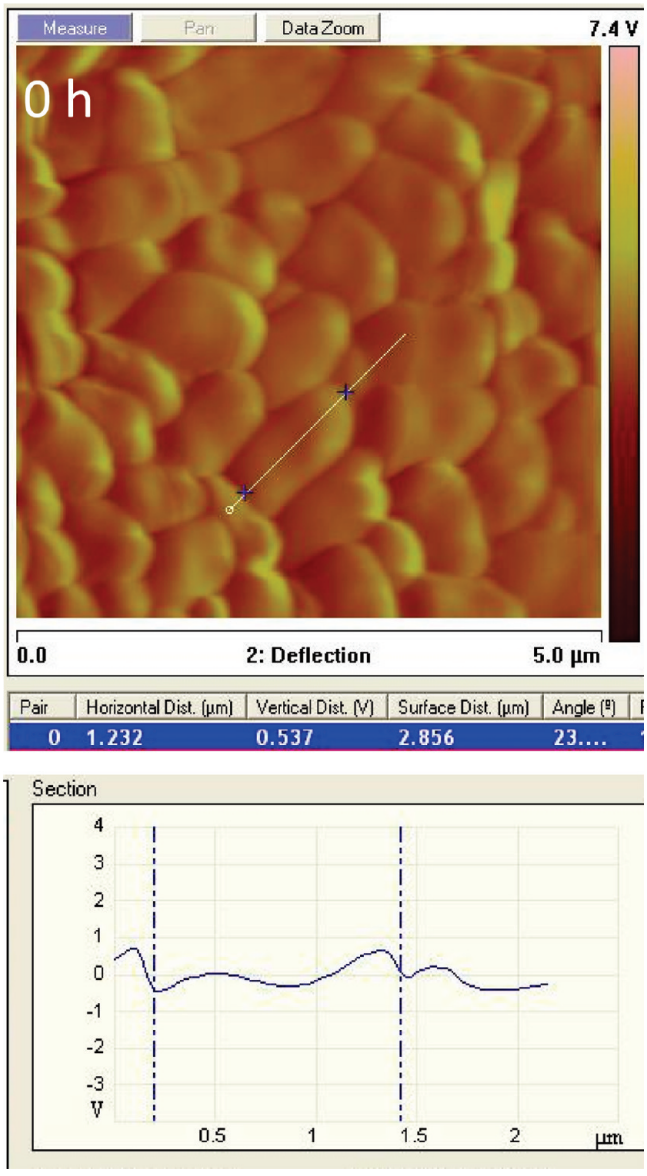

Figure 2. Deflection image of the untreated *Brevibacterium* cells (control i.e. 0 h) (before the Co_3O_4 nanoparticle synthesis) where the typical size of the *Brevibacterium* cells is calculated approximately as 1.2 μm (bottom panel).

other following various mechanisms to cope and survive by exhibiting sophisticated cooperative structural assemblies to behave like a multicellular organism. This organizational behavior, which is a protective mechanism shown by microbes (also observed by us in our earlier study on Co_3O_4 synthesis) while under stress, is mediated by the long-range biochemical interactions such as quoram sensing, chemotactic signaling, collective activation/deactivation of genes, and sometimes the exchange of genetic material.[32,33]

To further examine the effect of the exposure of the cells to the Co^{2+} ions (presence of exopolysaccharide at the cell surfaces leading to their aggregation as mentioned above and to see the change in their nanomechanical behavior due to the deformation) during the microbial synthesis, we performed force−distance spectroscopy on several cells taken from the synthesis both during the synthesis and after the synthesis was over. For this purpose, after getting the topography image (figure 3) and bringing the desired cell to the center of the frame, the force−distance data was collected at the center of each cell. The results on the cells treated with cobalt acetate (1 mM) for

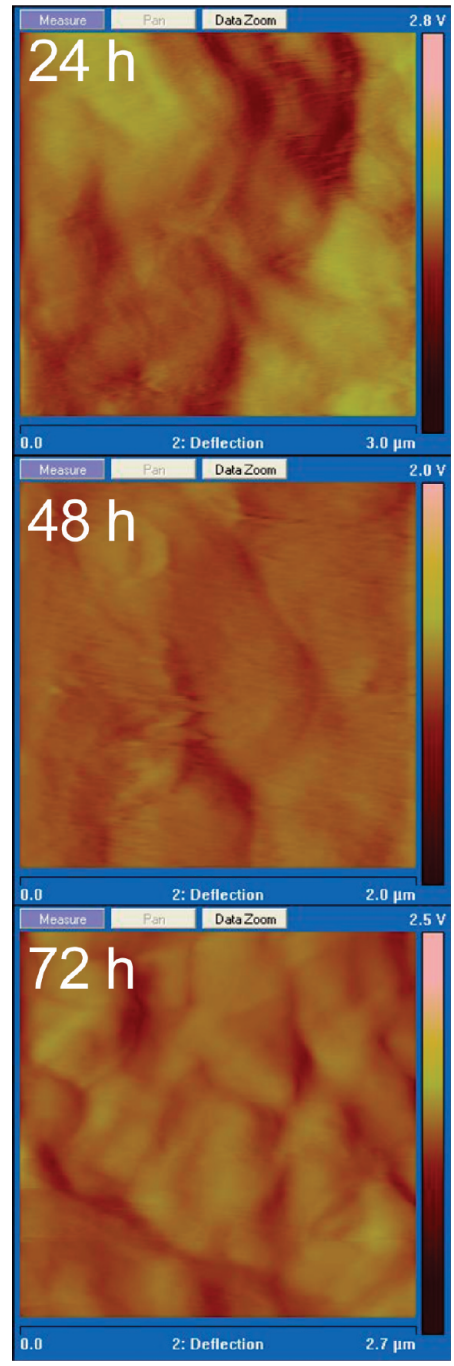

Figure 3. Deflection image of *Brevibacterium* cells after 24 h (top panel), 48 h (middle panel), and 72 h (bottom panel) during the Co_3O_4 nanoparticle synthesis.

24, 48, and 72 h are presented in Figure 4. Here, we kept the speed of loading and unloading at 598 nm/s, which is acceptable for the cellular systems. It should be noted that too high speed may lead to a distortion of the elastic response. The force−distance curves are also influenced by the interaction time and the load as well as by the physicochemical and mechanical changes of the cell surfaces by the cell immobilization. To take these factors into account, we also performed the force−distance measurements on the control (Figure 4, top-left panel) samples (untreated cells) and all the AFM parameters were kept unchanged (interaction time, protocol for cell immobilization, load, etc.). Here we used the spring-constant value of 1.86 N/m to convert the cantilever deflection (nm) versus tip−sample distance (nm) curves into the force (nN)−distance (nm) curves. The force

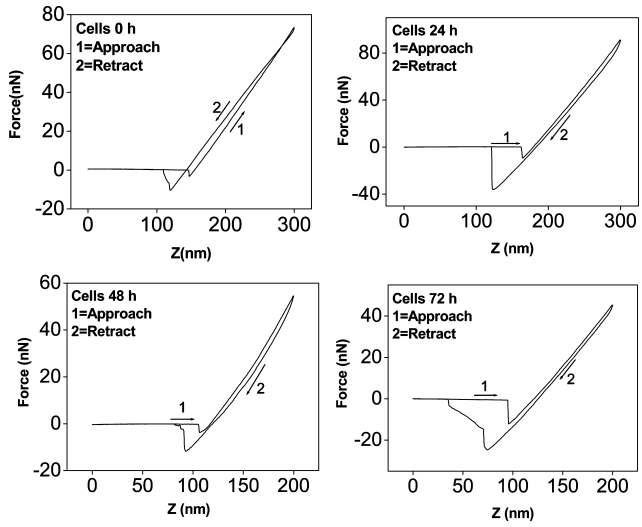

Figure 4. Force−distance curves on the cells obtained on treated *Brevibacterium* cells (0, 24, 48, and 72 h of the microbial synthesis of Co_3O_4 nanoparticles).

exerted on the sample during force measurements can be calculated using the relation

$$F = kd \tag{1}$$

where k is the spring constant of the cantilever and d is the deflection produced by the cantilever as a consequence of the interaction between the tip and the sample surface. The x-axis in these curves presents the distance traveled by the piezotube toward the sample, and the y-axis shows the force experienced by the cantilever after interacting with cells (in nano-Newtons). The details of the information provided by various parts of the force−distance curve (loading−unloading cycles) were discussed earlier in Figure 1. From the "contact" regions of all the force−distance curves shown in the Figure 4, it can be noticed that there is a significant difference between the approach and retract branches of the curves apart from being slightly nonlinear. For the ideal elastic surfaces (or hard surfaces), this deviation should not be there (no hysteresis in the contact region must be observed); that is, the approach and withdrawal contact lines must overlap and the retract curve should also cross the zero force level at the point where the approach curve touches the zero force point after jumping to contact the surface.[16] However, if the surface of the sample is plastically deformable then during the approach of the AFM tip, the sample undergoes a deformation, and in the retract cycle, the sample does not regain its original shape. It is considered that most of the samples show a mixed (plastic and elastic) behavior and the approach and retract curves rarely overlap on each other as seen in the present case. This can also happen due to a small hysteresis in the piezo in the z movement. In our case, the deviation in both the curves is due to the plasticity (irreversible deformation) of the cell surfaces, which is also visible from the indent left at the cell surface after the indentation. The best way to check the instrument related artifact is to do the force−distance curve measurements on the hard surface. We performed this measurement on the silicon surface and did observe only a small hysteresis in the contact region.[16] Therefore, we concluded that, in our case, the deviations in both the curves are primarily due to the plasticity (irreversible deformation) of the cell surfaces. Additionally, the fact that the retrace curve is falling behind the trace curve also proves the plastic behavior of cells. It should be noted that usually microbial cells do not show such type of behavior due to the presence of a rigid cell wall. However, in our case, due to the exposure to the metal ions during the microbial synthesis and due to the drying or dehydration during the sample preparation, the cells might show such type of plasticity at their surfaces. This is for the first time where a clear change in the topography of the microbial cells as well as their mechanical behavior has been observed during the synthesis of nanoparticles using microbes. The nonlinearity in the contact region is again the signature of the presence of the soft and deformable sample where the contact region of the curve is a convolution of the viscoelesatic properties of the sample with those of the cantilever, as for nondeformable tip or samples, the contact region should be perfectly linear.[34]

Another important feature in the curves presented in Figure 4 is the onset of the "jump-into the surface" region, which is characterized by the point where the gradient of the attractive force exceeds the spring constant.[16] This feature is due to the attractive forces such as capillary forces and van der Waals forces between the tip and the sample surface, which are mostly present under ambient conditions, as we discussed earlier. Some groups have reported not to see the "jump-to-contact" region in their force−distance curves on the bacterial cells. However, we believe that their observation is due to the dominant electrostatic repulsion where both the bacterial cells and the AFM tip were probably negatively charged, thereby masking the effect of the capillary forces.[35] In fact, in almost all the cases (normal relative humidity), the capillary forces are also strong enough to mask the van der Waals forces. The absolute linearity of the approach or retract curve in the noncontact region of the force curve shows the absence of any long-range attractive or repulsive forces in our case. Let us now discuss an additional hysteresis behavior in Figure 4, which is observed as a large difference in horizontal (Z) position of the jump-to-contact and jump-off contact points (also shown as regions 2 and 6 in the figure 1), which shows up due to the tip−sample interaction and is a signature of the presence of strong adhesion forces between tip and cellular surface probably originating from the exopolysaccharide and other biomolecules at the surface. In normal imaging, this adhesion loop is usually checked (on hard surface) to estimate the cleanliness of the tip, and it should be minimized. However, in the present case, we have used it to provide a quantitative evaluation of the variation of the adhesive forces at the cell surfaces during the exposure to the Co^{2+} ions in biosynthesis. In fact, the area under the adhesion loop (in the absence of Z-piezohysteresis) represents the work done in the approach−retract cycle against the tip−sample interaction. The amount of force required to snap the tip off the cell surface is given by the force just before the jump-off contact and gives a measurement of the maximum tip−sample adhesion. However, the measured adhesion force also depends on the time scale of the retraction; that is, the faster the curve, the lower the adhesion. In our case, the time taken for the retract curve was around 0.3 s, which is quite reasonable. The adhesive force calculated by the force plot comes out to be 10, 40, 15, and 25 nN after 0 h (control), 24 h, 48 h, and 72 h of exposure of the cells to metal ions during the microbial synthesis, respectively. We calculated the adhesion energy for various samples by calculating the area under the force−distance curve below the zero force line of the adhesion loop (refer to the schematic in Figure 1), and these values were 0 h $= -177.073 \times 10^{-18}$ J, 24 h $= -1211.45 \times 10^{-18}$ J, 48 h $= -197.01 \times 10^{-18}$ J, and 72 h $= -1067.49 \times 10^{-18}$ J. It is clear that the adhesive force and adhesive energy show an enhancement during the biosynthesis after the exposure of the bacterial cells to the metal ions, which

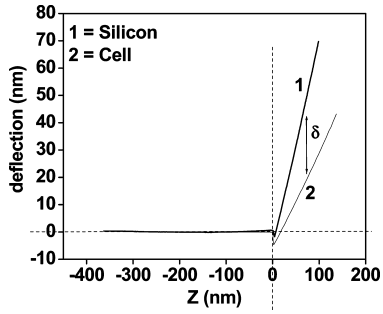

Figure 5. Schematic of the method used for the indentation depth calculation.

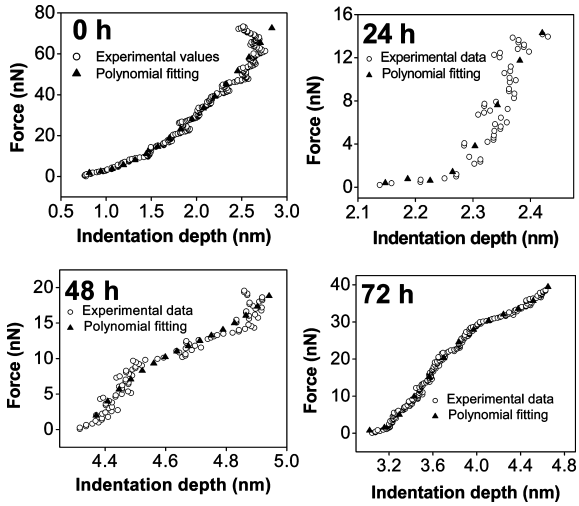

Figure 6. Curves showing the loading force as a function of indentation depth for 0 h, 24 h, 48 h, and 72 h of the reaction and their polynomial fits as calculated from the force−distance curves.

is probably due to the presence of an increasing amount of exopolysaccharide and other biomolecules at the surface as the microbial reaction proceeds.

To assess whether the cells have undergone physiological changes upon treatment with the cobalt acetate as reaction time evolves during the synthesis of Co_3O_4 nanoparticles, it is required now to do further quantitative analysis to calculate the indentation depth from the force spectroscopy data on the treated cells at 0, 24, 48, and 72 h. The indentation made by the tip on the cell surface during the force measurements is quantified by the indentation depth, δ, which can be calculated following the schematic shown in Figure 5 using the relation

$$\delta = d_1 - d_2 \tag{2}$$

where d_1 and d_2 correspond to the deflections produced by the approach curves on a hard surface such as silicon (where the indentation would be essentially zero) and a sample of interest, respectively.[26] In the schematic shown in Figure 5, we have explained the procedure that we followed to calculate the indentation depth at various load values in the contact region. In this method, as a first step, the offsets in the deflection and the stresses on the cantilever were taken into consideration. In the second step, the point at which jump into contact occurs due to the instability between the tip and the sample is made common for both the silicon reference and the sample, as shown in the schematic (Figure 5). In Figure 6, we have plotted the indentation depth vs force curves (cantilever deflection) for various time-scales of Co^{2+} ion exposure during the synthesis. It is clear that the indentation depth inside the cells generally

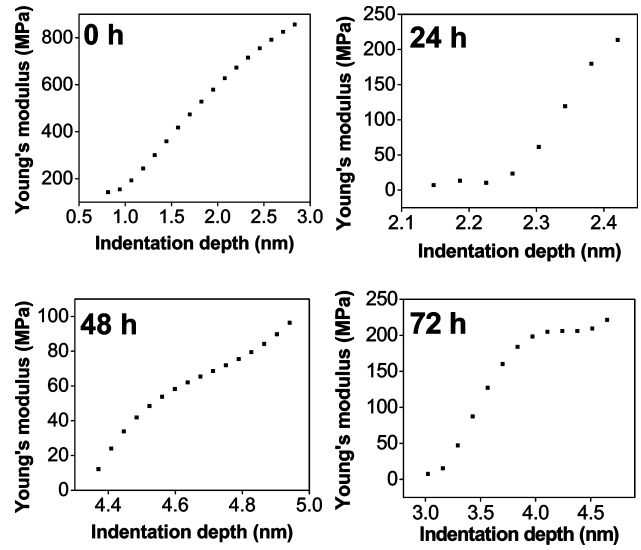

Figure 7. Curves showing typical Young's modulus values as a function of indentation depth calculated using the Hertz model for 0 h, 24 h, 48 h, and 72 h of the reaction.

increases with increasing force applied at the cell surface. It is interesting to know however that, for a typical applied force (say 10 nN), the indentation depth calculated for the untreated cells (0 h) is smallest and the indentation depth shows an overall increasing trend as the reaction progresses, which is probably due to an overall decrease in the stiffness of the cell surface during the synthesis as the exposure time to the metal ions increases. These results clearly indicate a sharp change in the nanomechanical properties of cells after exposing them to the toxic environment of transition metal ions.

As already mentioned, the nanomechanical properties of cells such as Young's modulus are extremely sensitive to the surrounding environment; therefore, next, we calculated the Young's modulus values for each of the samples before, during, and after the synthesis (various levels of exposure to the metal ions) using the Hertz model.[36,37] A more generalized model given by Sneddon et al. is an extension of the Hertz model which takes into account the contribution from the deformable tip.[26] The Hertz model is a good choice for calculating the Young's modulus of the cells, as this model assumes that it is the sample alone undergoing deformation during the tip−sample interaction rather than the tip itself which is very stiff in comparison to the biological material, as the Young's modulus for the AFM tips for silicon or silicon nitride is several orders of magnitude higher than that for cells. Assuming the tip shape to be spherical or paraboloid, the Young's modulus, E, according to the Hertz model is given by the relation

$$E = \frac{3F(1 - \sigma^2)}{4R^{1/2}\delta^{3/2}} \tag{3}$$

where F is the force experienced by the cantilever and the indentation depth, δ, can be obtained from eqs 1 and 2, respectively. R is the radius of curvature of the tip used for the force measurement (estimated to be around 100 nm), and σ is Poisson's ratio. The value of Poisson's ratio always comes in the range from 0 to 0.5, but for the biological cells, σ typically lies in a range from 0.3 to 0.5.[37,38] In the present case, we have taken Poisson's ratio as 0.5, assuming the cells to be incompressible during the force measurements. In Figure 7, we have shown the calculated values of the Young's modulus using eq 3 at various levels of reaction as a function of indentation depth.

It should be noted that as the biological cells are inhomogeneous systems the elastic properties vary with the indentation depth of the material. From Figure 7, we infer that for the control sample (0 h) the Young's modulus shows a gradual increase as a function of indentation depth as compared to the rest of the curves (for 24, 48, and 72 h after the reaction starts). It is also evident that, at larger indentation depth values, we see an approach toward a plateau in the Young's modulus values almost for all the four cases, which is usually the situation when the applied load is proportional to the deformation produced in the sample, indicating that the region is in the elastic limit. In this region, the calculated values for Young's modulus for 0, 24, 48, and 72 h of reaction are 769.28 ± 73.07 MPa, 170.921 ± 38.93 MPa, 82.860 ± 20.42 MPa, and 209.526 ± 6.14 MPa, respectively, which shows mostly a decreasing trend in elasticity of the cells as the reaction progresses. As we discussed earlier, it is believed that the Young's modulus of a cell surface may originate from various sources such as (a) the cell wall itself and/or (b) underlying structures (cytoskeleton etc.) and/or (c) a pressure difference between the cell interior and the exterior (turgor pressure). The biochemical process inside the cells and at the cell surface might be greatly affected by the presence of Co^{2+} ions, leading to the loss of turgor pressure and change in the elastic properties of the cell wall itself as well. As seen in the topographical images of the cells, we can conclude that these factors collectively lead to an overall drop in the elasticity of the cells in our case, although the approach to the plateau of Young's modulus as a function of indentation depth is faster in the 0 and 24 h samples. This saturation point is different for each sample depending upon their exposure to the Co^{2+} ions, probably due to the clumping of cells during the microbial synthesis. Unexpected high values of Young's modulus for the 0 h sample (before reaction) indicate that the Turgor pressure is maintained. As the reaction progresses, we notice a decrease in the Young's modulus values and softness of the sample, which is probably due to turgid loss during the synthesis process.

In summary, our force−spectroscopy measurements on the microbial results show an overall decrease in the Young's modulus value on the marine bacterium cells and an increase in the adhesiveness due to the secretion of the proteins and other biomolecules at the cell surfaces during interaction of the cells with the Coacetate during the synthesis of Co_3O_4 nanoparticles. We believe that this is the first of its kind of study where a detailed quantitative and qualitative analysis (before, during, and after the microbial synthesis) indicates the sensitivity of the micromechanical properties of cells to the surrounding toxic environment.

Acknowledgment. One of the authors, P.P., acknowledges the financial support by the Department of Science and Technology, India, through Grant No. SR/S5/NM-104/2006 under the Nano Mission program to carry-out this work. K.V. also acknowledges the support from the same grant to support his project-assistantship. U.K. acknowledges the support from the Council of Scientific and Industrial Research, India (CSIR), for providing the Senior Research Fellowship. The authors also thank Baishakhi Mazumder for his help with the manuscript.

References and Notes

(1) Kumar, U.; Shete, A.; Harle, A. S.; Kasyutich, O.; Schwarzacher, W.; Pundle, A.; Poddar, P. *Chem. Mater.* **2008**, *20* (4), 1484–1491.

(2) Bansal, V.; Poddar, P.; Ahmad, A.; Sastry, M. *J. Am. Chem. Soc.* **2006**, *128* (36), 11958–11963.

(3) Mazumder, B.; Uddin, I.; Khan, S.; Ravi, V.; Selvraj, K.; Poddar, P.; Ahmad, A. *J. Mater. Chem.* **2007**, *17*, 3910–3914.

(4) Uddin, I.; Adyanthaya, S.; Syed, A.; Selvaraj, K.; Ahmad, A.; Poddar, P. *J. Nanosci. Nanotechnol.* **2008**, *8* (8), 3909–3913.

(5) Kowshik, M.; Ashtaputre, S.; Kharrazi, S.; Vogel, W.; Urban, J.; Kulkarni, S. K.; Paknikar, K. M. Nanotechnology 2003, *14* (1), PII S0957-4484(03)39921-0.

(6) Bansal, V.; Rautaray, D.; Bharde, A.; Ahire, K.; Sanyal, A.; Ahmad, A.; Sastry, M. *J. Mater. Chem.* **2005**, *15* (26), 2583–2589.

(7) Bansal, V.; Rautaray, D.; Ahmad, A.; Sastry, M. *J. Mater. Chem.* **2004**, *14* (22), 3303–3305.

(8) Bharde, A.; Wani, A.; Shouche, Y.; Joy, P. A.; Prasad, B. L. V.; Sastry, M. *J. Am. Chem. Soc.* **2005**, *127* (26), 9326–9327.

(9) Li, X.; Logan, B. E. *Langmuir* **2004**, *20* (20), 8817–8822.

(10) Velegol, S. B.; Logan, B. E. *Langmuir* **2002**, *18* (13), 5256–5262.

(11) Butt, H. J.; Cappella, B.; Kappl, M. *Surf. Sci. Rep.* **2005**, *59* (1−6), 1–152.

(12) Binnig, G.; Quate, C.; Gerber, G. *Phys. Rev. Lett.* **1986**, *56*, 930–933.

(13) Binnig, G.; Rohrer, H. *Helv. Phys. Acta* **1982**, *55*, 726–735.

(14) Ralston, J.; Larson, I.; Rutland, M. W.; Feiler, A. A.; Kleijn, M. *Pure Appl. Chem.* **2005**, *77* (12), 2149–2170.

(15) Burnham, N. A.; Colton, R. J. *J. Vacuum Sci. Technol. A* **1989**, *7*, 2906.

(16) Weisenhorn, A. L.; Khorsandi, M.; Kasas, S.; Gotzos, V.; Butt, H. *Nanotechnology* **1993**, *4*, 106–113.

(17) Radmacher, M.; Fritz, M.; Kacher, C. M.; Cleveland, J. P.; Hansma, P. K. *Biophys. J.* **1996**, *70* (1), 556–567.

(18) Tomasetti, E.; Legras, R.; Nysten, B. *Nanotechnology* **1998**, *9*, 305–315.

(19) Rotsch, C.; Jacobson, K.; Radmacher, M. *Proc. Natl. Acad. Sci. U.S.A.* **1999**, *96* (3), 921–926.

(20) Matzke, R.; Jacobson, K.; Radmacher, M. *Nat. Cell Biol.* **2001**, *3* (6), 607–610.

(21) Radmacher, M. *At. Force Microsc. Cell Biol.* **2002**, *68*, 67–90.

(22) Arnoldi, M.; Fritz, M.; Bauerlein, E.; Radmacher, M.; Sackmann, E.; Boulbitch, A. *Phys. Rev. E* **2000**, *62* (1), 1034–1044.

(23) Braet, F.; Rotsch, C.; Wisse, E.; Radmacher, M. *Appl. Phys. A: Mater. Sci. Proc.* **1998**, *66*, S575–S578.

(24) Xu, W.; Mulhern, P. J.; Blackford, B. L.; Jericho, M. H.; Firtel, M.; Beveridge, T. J. *J. Bacteriol.* **1996**, *178* (11), 3106–3112.

(25) Cross, S. E.; Jin, Y. S.; Rao, J.; Gimzewski, J. K. *Nat. Nanotechnol.* **2007**, *2* (12), 780–783.

(26) Touhami, A.; Nysten, B.; Dufrene, Y. F. *Langmuir* **2003**, *19* (11), 4539–4543.

(27) Levy, R.; Maaloum, M. Nanotechnology 2002, *13* (1), PII S0957-4484(02)27598-4.

(28) Hutter, J. L.; Bechhoefer, J. *Rev. Sci. Instrum.* **1993**, *64* (11), 3342–3342.

(29) Zhang, Y.; Jock, S.; Geider, K. *Mol. Gen. Genet.* **2001**, *264* (5), 732–733.

(30) Richau, J. A.; Choquenet, D.; Fialho, A. M.; SaCorreia, I. *Res. Microbiol.* **1997**, *148* (3), 251–261.

(31) Tang, Y. J. J.; Ashcroft, J. M.; Chen, D.; Min, G. W.; Kim, C. H.; Murkhejee, B.; Larabell, C.; Keasling, J. D.; Chen, F. Q. F. *Nano Lett.* **2007**, *7* (3), 754–760.

(32) Ben Jacob, E.; Becker, I.; Shapira, Y.; Levine, H. *Trends Microbiol.* **2004**, *12* (8), 366–372.

(33) Ben-Jacob, E.; Cohen, I.; Golding, I.; Gutnick, D. L.; Tcherpakov, M.; Helbing, D.; Ron, I. G. *Physica A: Statistical Mechanics and Its Applications* **2000**, *282* (1−2), 247–282.

(34) A-Hassan, E.; Heinz, W. F.; Antonik, M. D.; D'Costa, N. P.; Nageswaran, S.; Schoenenberger, C. A.; Hoh, J. H. *Biophys. J.* **1998**, *74* (3), 1564–1578.

(35) Burks, G. A.; Velegol, S. B.; Paramonova, E.; Lindenmuth, B. E.; Feick, J. D.; Logan, B. E. *Langmuir* **2003**, *19* (6), 2366–2371.

(36) Brochu, H.; Vermette, P. *Langmuir* **2008**, *24* (5), 2009–2014.

(37) Dulinska, I.; Targosz, M.; Strojny, W.; Lekka, M.; Czuba, P.; Balwierz, W.; Szymonski, M. *J. Biochem. Biophys. Methods* **2006**, *66* (1−3), 1–11.

(38) Dimitriadis, E. K.; Horkay, F.; Maresca, J.; Kachar, B.; Chadwick, R. S. *Biophys. J.* **2002**, *82* (5), 2798–2810.

JP902698N